Polymer 290 (2024) 126494

Contents lists available at ScienceDirect

Polymer

journal homepage: www.elsevier.com/locate/polymer

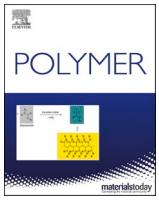

Titanium-catalyzed synthesis of polymyrcene and polyanethol and application as sustainable additives for poly(lactic acid)

Joan Vinueza-Vaca [a,b], Emma Franco-Mateo [a,b,c], Valentina Sessini [a,b], Marta E. G. Mosquera [a,b], Virginia Souza-Egipsy [c], Javier Ramos [c,d], Juan F. Vega [c,d], Gerardo Jiménez [a,b,**], Vanessa Tabernero [a,b,*]

[a] Department of Organic and Inorganic Chemistry., Alcalá University, Campus Universitario, 28871, Alcalá de Henares, Spain
[b] Insitute of Chemical Research Andrés M. del Rio, IQAR, Alcalá de Henares, Spain
[c] BIOPHYM, Departamento de Física Macromolecular, Instituto de Estructura de la Materia, IEM-CSIC, c/Serrano 113 bis, 28006, Madrid, Spain
[d] Interdisciplinary Platform for Sustainable Plastics towards a Circular Economy, SUSPLAST-CSIC, 28006, Madrid, Spain

A B S T R A C T

The replacement of fossil-derived plastics with those obtained from bio-based resources, which present suitable performance to be employed as commodity plastics is currently an important field of research, given the urgent need to transition from a fossil-based to a more sustainable economy. In this context, this work is focused on the application of a catalytic system based on silsesquioxane-cyclopentadienyl titanium complexes for the preparation of bio-based polymers, which can be used as additives to improve the poor material properties of a biodegradable polymer such as poly(lactic acid) (PLA). These titanium complexes, when activated with methylaluminoxane or with triflate salts, are shown to be capable of the polymerization of two bio-based monomers: myrcene and anethole. It is notable that polymerizations with these two distinct monomers take place through different mechanisms. The resulting polymyrcene (PMy) and polyanethol (PAN) have been applied as modifiers for PLA. Binary blends of PMy and PLA exhibited a considerable decrease in T_g and the promotion of PLA crystallization for a PMy content below 15 wt%. The mechanical properties of the PLA/PMy blends also displayed plasticization, with a decrease in the elastic modulus and enhanced plasticity, which resulted in less fragile systems compared to pure PLA. Morphological analysis has indicated a partially miscible, phase-separated system with micron-sized domains. In contrast, PAN completely inhibited PLA crystallization and the PLA/PAN blends were immiscible, but well-dispersed, a phase-separated system was obtained in solvent-casting film preparation with very small PAN domains. The blends showed higher tensile modulus than pure PLA and an absence of plastic behaviour, resulting in more fragile systems upon the addition of PAN to PLA.

1. Introduction

The production and disposal of fossil-based plastics is widely recognized as a significant environmental problem worldwide. To partly address this issue, there has been a growing trend in recent years towards the use of renewable feedstocks as a more sustainable source for polymer production [1]. Polylactide (PLA), a biodegradable and low-cost polymer derived from sugarcane, has attracted significant attention as a potential alternative to traditional fossil-based plastics. PLA has several advantages, including biodegradability and a reduced carbon footprint, making it a promising option for a wide range of applications, such as packaging, textiles, and medical implants. As the demand for environmentally friendly materials continues to grow, the development and utilization of sustainable polymers like PLA will play an increasingly important role in reducing the environmental impact of plastic production and waste. Although PLA is one of the most promising alternatives to fossil-based plastics, its mechanical properties and processability are not always optimal, so an important goal is to improve them by the addition of suitable additives during processing and manufacturing. To address these challenges, researchers have investigated the use of a range of additives, including plasticizers, impact modifiers, and fillers, with the aim of enhancing the properties of PLA and expanding its range of applications [2,3].

Myrcene is a terpene (Fig. 1, left) found in essential oils of plants such as dill, thyme, and rosemary, that has a structure like butadiene, and its polymerization can provide polymyrcene (PMy) which has similar elastic properties to those shown by polybutadiene, and therefore it can be considered a bio-based elastomer. β-myrcene has previously been

* Corresponding author. Department of Organic and Inorganic Chemistry, Alcalá University, Campus Universitario, 28871, Alcalá de Henares, Spain.
** Corresponding author. Department of Organic and Inorganic Chemistry, Alcalá University, Campus Universitario, 28871, Alcalá de Henares, Spain.
E-mail addresses: joan.vinueza@edu.uah.es (J. Vinueza-Vaca), emma.franco@csic.es (E. Franco-Mateo), valentina.sessini@uah.es (V. Sessini), martaeg.mosquera@uah.es (M.E. G. Mosquera), virginia.souza-egipsy@csic.es (V. Souza-Egipsy), j.ramos@csic.es (J. Ramos), jf.vega@csic.es (J.F. Vega), gerardo.jimenez@uah.es (G. Jiménez), vanessa.tabernero@uah.es (V. Tabernero).

https://doi.org/10.1016/j.polymer.2023.126494
Received 20 June 2023; Received in revised form 11 October 2023; Accepted 12 November 2023
Available online 18 November 2023

studied as a monomer or comonomer for anionic [4,5] and radical polymerizations [6]. However, to date, few reports describe controlled polymerization of this monomer [7–11], achieving stereospecific polymerization of β-myrcene. These limited contributions are mainly based on lanthanide catalytic systems [12–14]. Meanwhile, anethol is an aromatic compound (Fig. 1, right) found in anise, fennel, and star anise, that contains a vinylic functionality and a *p*-methoxy group. The corresponding polymer that can be obtained has a polystyrene structure but with pendant polar functional groups, making the polymerization of this substrate highly interesting. However, to the best of our knowledge, reports relating to successful homopolymerization of anethol are rather scarce to date [15].

In view of the excellent behavior previously shown by the monocyclopentadienyl titanium compounds in catalysts [16,17], we sought to apply these robust silsesquioxane-cyclopentadienyl titanium complexes, [Ti(h^5-$C_5H_4SiMe_2OPh_7Si_7O_{11}$-k^2$O_2$)Cl] (**1**) [18,19] (Fig. 2), as pre-catalysts for the polymerization of both myrcene and anethol, through either a Ziegler-Natta or a cationic mechanism, respectively. The geometric and stability properties of **1** make it an excellent candidate for controlled polymerization processes and, therefore to obtain polymers with a significant potential for manufacturing valuable bio-based polymeric products, which is the primary target on the gradually replacement of the fossil-based polymers. Furthermore, it is foreseen that any oligomers obtained could be used as additives to improve the properties of other materials such as PLA [20,21].

In this study, we report the results obtained from the polymerization of myrcene and anethole using the silsesquioxane-cyclopentadienyl titanium complex, [Ti(η^5-$C_5H_4SiMe_2OPh_7Si_7O_{11}$-κ^2$O_2$)Cl] as pre-catalyst (Fig. 2). The resulting polymers have been fully characterized whilst their potential as additives for improving the properties of PLA has been evaluated, with the morphological and mechanical properties of the resulting blends studied. The relevance of the results achieved could provide new insights into the controlled polymerization of bio-based monomers and the application of the resulting polymers to generate valuable bio-based polymeric products.

2. Experimental section

2.1. General procedures and materials

Air- and moisture-sensitive compounds were manipulated under an argon atmosphere using standard Schlenk techniques or in an MBraun glovebox. All glassware was stored in an oven at 80 °C prior to use.

Modified methylaluminoxane (MMAO; 7 wt% solution in toluene; Merck) was used as received. β-myrcene (≥95%) and anethole was purchased from Merck and used after distillation. The titanium complex [Ti(η^5-$C_5H_4SiMe_2OPh_7Si_7O_{11}$-κ^2$O_2$)Cl] (**1**) was synthesized as previously described in the literature [22]. $AgSO_3CF_3$ and $SiMe_3SO_3CF_3$ were purchased from Fisher Scientific and used as received.

Poly(lactic acid) (PLA) 2003D, with a density of 1.24 g cm^{-3}, a molecular weight (M_w) of ca. 2.3 × 10^5 g mol^{-1}, and a Melt Flow Index (MFI) of 6 g · 10 min^{-1} (210 °C, 2.16 kg) was supplied by Nature Works®, USA and was used as received.

Microanalyses (C,H, N, S) were performed on PerkinElmer CHNS/O 2400 or Leco CHNS-932 microanalyzers.

^{1}H and ^{13}C NMR spectra were recorded at 25 °C with a Bruker AV400 spectrometer (^{1}H NMR at 400 MHz, ^{13}CNMR at 100.6 MHz, ^{29}Si NMR at 79.5 MHz, ^{19}F NMR at 376.4 MHz), using 5 mm (o.d.) NMR tubes. Chemical shifts were referenced to TMS and calculated using the residual isotopic impurities of the deuterated solvent ($CDCl_3$: $\delta = 7.26$ ppm in ^{1}H NMR and $\delta = 77.17$ ppm in ^{13}C NMR experiments).

The number-average and weight-average molar masses (M_n and M_w, respectively) and polydispersities (Đ) of the polymer samples were determined by Size Exclusion Chromatography (SEC) at 35 °C with a 1260 Infinity II high-speed liquid chromatography system (Agilent). Tetrahydrofuran (THF) was used as the eluent and the flow rate was set as 1.0 mL min^{-1}. Two Mixed D columns in series were used. Calibrations were performed using polystyrene standards.

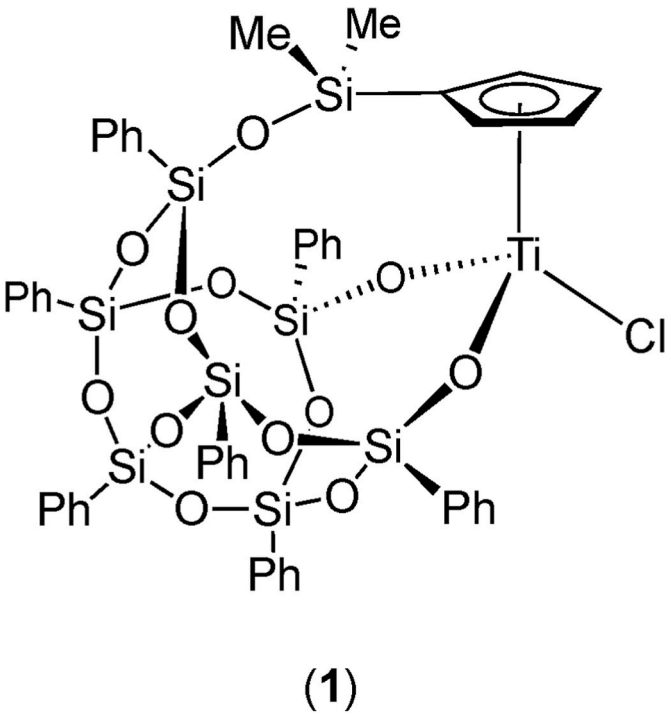

Fig. 2. Silsesquioxane-cyclopentadienyl titanium complex (**1**) employed in this study.

2.2. Preparation of [Ti(η^5-$C_5H_4SiMe_2OPh_7Si_7O_{11}$-κ^2$O_2$)][$SO_3CF_3$] (2)

a) To a mixture of 0.6 g of [Ti(η^5-$C_5H_4SiMe_2OPh_7Si_7O_{11}$-κ^2$O_2$)Cl] (0.53 mmol) and 0.14 g of $AgSO_3CF_3$ (0.54 mmol) were added 30 mL of dried CH_2Cl_2, and the reaction mixture was vigorously stirred overnight. The resulting suspension was filtered over celite, the solvent was removed under vacuum and the residue was washed with *n*-hexane (10 mL) to afford **2** as a greenish yellow solid in 89 % yield (0.59 g, 0.47 mmol).

Fig. 1. Monomers used in this study.

b) $SiMe_3SO_3CF_3$ (0.2 mL, 1.10 mmol) was added to a solution of **1** (1.25 g, 1.10 mmol) in toluene (30 mL) at room temperature using a syringe. The solution was stirred until gas release was complete. The formed solid was collected by filtration and washed with *n*-hexane (2 × 30 mL) to provide **2** as a greenish yellow solid in 90 % yield (1.1 g, 0.88 mmol). $C_{50}H_{45}F_3O_{15}SSi_8Ti$ (1246): calcd. C, 48.14; H, 3.64; O, 19.24; S, 2.57; found C, 47.96; H, 3.61; O, 19.31; S, 2.58. ^{1}H NMR ($CDCl_3$): δ 0.53 (s, 6 H, $SiMe_2$), 7.12, 7.26 (m, 2 × 2 H, C_5H_4), 7.37 (m, 7 H, Ph), 7.48 (m, 7H, Ph-POSS), 7.70 (m, 14 H, Ph). $^{13}C\{^1H\}$ NMR ($CDCl_3$): δ 1.70 ($SiMe_2$), 126.2, 126.3, 124.4 (C_5H_4), 127.84, 127.89, 127.90, 127.92, 127.95, 130.04, 130.29, 130.41, 130.46, 130.55, 130.64, 130.67, 130.78, 130.82, 130.89, 130.96, 133.97, 133.99, 134.08, 134.16, 134.22 (Ph). ^{1}H–^{29}Si HMBC: δ −2.1 ppm ($SiMe_2$), 77, 78, 79 (Si-POSS). ^{19}F NMR ($CDCl_3$): δ −76 (CF_3)

2.3. Polymerization experiments

2.3.1. Homopolymerization of myrcene

2.3.1.1. A standard polymerization test is described. To 30 mL of a solution of MMAO-12 (7 wt%) in toluene was added myrcene until a final volume of 55 mL was reached. The mixture was heated to the required temperature for 10 min, whilst being vigorously stirred. Then, a solution of the catalyst in toluene (5 mL), containing the required amount of **1**, was added. The reaction was stirred for 1 h, at this temperature. The reaction was then quenched by adding 180 mL of an acidified solution of methanol (with 1% of BHT). The polymer was recovered by decantation and purified through several cycles of dissolution in diethyl ether and precipitation by adding methanol. Finally, the solvent was removed under vacuum until a constant weight was obtained. All reactions were performed using a monomer concentration of 0.6 M in toluene. ^{1}H NMR of polymyrcene ($CDCl_3$): δ 1.62 (9, 9′-H), 1.69 (6H, 10, 10′-H), 2.05 (16H, 1, 1′, 4, 4′, 5, 5′, 6, 6′-H), 5.14 (4H, 3, 7, 3′, 7′-H).

^{13}C NMR of polymyrcene ($CDCl_3$): δ 25.70 [10, 10′-C], 17.70 [9, 9′-C], 26.97 [4, 6, 4′, 6′-C], 30.42 [1, 1′-C], 37.09 [5, 5′-C], 131.41 [8, 8′-C], 124.43 [3, 7, 3′, 7′-C], 139.01 [2, 2′-C].

2.3.2. Homopolymerization of anethol

A flask fitted with a septum was charged, inside of a glove box, with 0.27 g of [Ti(η^5-$C_5H_4SiMe_2OR_7Si_7O_{11}$-$\kappa^2O_2$)][$SO_3CF_3$] (0.216 mmol) and to this was added 20 mL of dry CH_2Cl_2. Outside of the dry box, the solution was cooled to −78 °C and 8 mL of anethole (54.15 mmol) were syringed into the flask. The cooling bath was removed, and the mixture was allowed to come to room temperature while the reaction was stirred. The reaction mixture was stirred at room temperature for the indicated time and then the reaction was quenched by the addition of 100 mL of wet ethanol, and the precipitated polymer was recovered by filtration. The crude polyanethol was then dissolved in toluene and precipitated by adding ethanol until a white solid was obtained. All the reactions were performed at a monomer concentration of 2 M in CH_2Cl_2.

2.4. Preparation of the blends and characterization methods

PLA/PAN and PLA/PMy blends were prepared by dissolving the polymers in $CHCl_3$. PAN and PMy, used as bio-based additives, were added to the PLA matrix at different concentrations. In Table 1 the different blends formulations are reported. The thin films were obtained by a solvent casting method in a glass Petri dish and evaporated at room temperature under ventilation for 24 h to obtain films with a thickness of around 120–150 μm. The obtained samples were named emphasizing the respective PAN or PMy content. A pure PLA sample was prepared in the same way for comparison.

The thermal properties of pure polymers and blends were obtained by Differential Scanning Calorimetry (DSC) analysis and by Thermogravimetric Analysis (TGA). Glass transition temperatures (T_g), cold crystallization and melting temperatures were obtained using a DSC7 (PerkinElmer) under an ultra-high purity N_2 atmosphere. Samples were encapsulated in aluminium pans, sealed and heated from 20 °C to 220 °C at 10 °C·min^{-1}. Cooling and subsequent heating scans were also registered. The crystallinity X_c of the samples was obtained from the difference between the corresponding melting, ΔH_m, and the cold-crystallization, ΔH_{cc}, enthalpies, using the enthalpy of a 100% crystalline PLA polymer, $\Delta H_m^0 = 93{,}6$ J g^{-1}, and accounting in each case for the effective amount of PLA in the blend [23]. The TGA measurements were carried out using a TGA55 analyzer (TA Instruments). The dynamic experiments were performed using around 10 mg of sample from room temperature to 600 °C at 10 °C·min^{-1} under a nitrogen atmosphere (flow rate of 60 mL min^{-1}). The initial degradation temperatures ($T_{5\%}$) were determined at 5% mass loss while temperatures at the maximum degradation rate (T_{max}) were calculated from the first derivative of the TGA curves (DTG).

Table 1
Formulations of PLA/PAN and PLA/PMy blends.

Sample	PLA (wt%)	PAN2 (wt%)	PMy (wt%)
PLA	100	–	–
PLA5PAN	95	5	–
PLA15PAN	85	15	–
PLA20PAN	80	20	–
PLA2PMy	98	–	2
PLA5PMy	95	–	5
PLA7PMy	93	–	7
PLA10PMy	90	–	10
PLA12.5PMy	87.5	–	12.5
PLA15PMy	85	–	15

The compatibility of the polymers as well as the morphology of the samples previously sputter-coated with gold (Polaron SEM coating system, 1.4 kV–1.8 mA – 120 min, thickness » 500 Å) was studied by Scanning Electron Microscopy (ZEISS DSM-950 instrument) operating at 15 kV. The polymeric blends were frozen using liquid N_2 and then cryo-fractured to obtain the SEM micrographs of the fracture surface before and after etching with xylene and hexane overnight at room temperature for PLA/PAN and PLA/PMy blends, respectively.

A PerkinElmer dynamic mechanical analyser DMA7 in the film extensional mode was used. The dynamic stress for different values of dynamic strain between 0.01 and 0.25 % at a frequency of 1 Hz and room temperature were obtained. The results obtained in the linear viscoelastic region allowed for measurement of the complex extensional modulus, E*, that it has been reported to be highly correlated to the Young modulus in different types of materials and composites [24]. For this investigation, rectangular shaped samples of about 10 mm × 5 mm × 0.150 mm were cut from the films prepared from solution as described above.

Morphological features were studied using Polarized Optical Microscopy (POM) and contact mode Atomic Force Microscopy (AFM) imaging of selected films fully crystalized at 120 °C. For POM a Nikon Eclipse E600POL equipped with a digital camera DXM1200 has been used, and for AFM imaging with a μTA™ 2990 Micro-Thermal Analyzer has been performed. V-shaped silicon nitride probes with cantilever length of 200 μm and a spring constant of 0.032 N m^{-1} was used. For the morphological observations the polymeric films were supported on glass wafers.

3. Results and discussion

The silsesquioxane-cyclopentadienyl compound [Ti(η^5-$C_5H_4SiMe_2OPh_7Si_7O_{11}$-$\kappa^2O_2$)Cl] (**1**) was synthesized as previously described [22]. This compound has been shown to be a very active system for oxidation of different substrates using aqueous hydrogen peroxide as primary oxidant. These excellent catalytic properties have been attributed to the hydrophobic pocket that the

silsesquioxane-cyclopentadienyl ligand generates around the titanium atom, which also protects it from adventitious impurities and allow us it to be handle under air. This aspect, together with the well-known catalytic properties of monocyclopentadienyl complexes, prompted us to study its catalytic behaviour with the two bio-based monomers mentioned above; β-myrcene and anethol.

Firstly, we studied the homopolymerization of β-myrcene in toluene, using the [Ti(η^5-$C_5H_4SiMe_2OPh_7Si_7O_{11}$-$\kappa^2O_2$)Cl] complex, (**1**), as pre-catalyst, assisted by MMAO as co-catalyst (Table 2). To optimize the polymerization conditions, initially a molar ratio of 1(**1**):500 (**MMAO**):500(**My**) was selected, modifying the temperature to investigate its effect, since it is well established that the temperature may affect both the process activity and the final polymer molecular weight. Different catalytic tests were carried out at 25, 80, and 130 °C. The results confirmed a reduction in the polymer molecular weight as the temperature increases (Table 2, entries 1, 2 and 3), which indicates that a chain transfer processes to the Al centers of the co-catalyst are more favored than the propagation reaction. Therefore, the obtained results confirmed the influence of the temperature on the activity, reaching an optimal activity at 80 °C since, both at 25 and at 130 °C the yield is significantly lower.

Once 80 °C was established as the optimal temperature, the influence of the monomer molar ratio was studied, observing that it had a significant effect on both the catalyst activity and the molecular weights of the resulting polymers. Doubling the myrcene/[Ti] molar ratio resulted in a dramatic decrease in catalytic activity (Table 2, entry 5 *vs*. 6). After this part of the study, the optimal catalyst/monomer molar ratio was set at 1/250. The next experimental parameter studied was the catalyst/co-catalyst ratio (Table 2, entries 5 and 7).When the catalyst/co-catalyst molar ratio was increased from 1:250 to 1:500, the yield was reduced by around three times. As a result of this complete study, the optimal polymerization conditions for myrcene using the catalytic system were selected as 80 °C, 1 h of reaction time, and a molar ratio of 1(**1**):250 (MAO):250(My).

The polymeric materials obtained were readily soluble in THF, which suggests that there is extremely limited or no cross-linking of the polymer chains. In all cases, NMR studies are in accordance with a predominant 1,4- stereoregularity (90%; *cis*- ≈ 75% and *trans*- ≈ 25%) *vs*. a 3,4- stereoregularity (10%). The signals in the range 5.0–5.2 ppm were assigned as the olefinic protons of the 1,4-units (*cis*- and *trans*-), whereas the two doublets at 4.73 and 4.76 ppm to the olefinic protons of the 3,4-units. Size exclusion chromatography (SEC) results for these polymers showed large PDI values. All these observations are in accordance with typical Ziegler-Natta behavior, as previously reported for similar catalyst systems with other olefins [14].

Meanwhile, the catalytic system **1**/MMAO was found to be completely inactive for anethol polymerization, independent of the reaction conditions applied. As a result of this inactivity, we attempted a different strategy. Taking into account that anethol polymerization mainly takes place through a cationic mechanism and that triflate complexes of titanium have been described as suitable catalysts in related catalytic processes [25], new cationic triflate derivative of [Ti(η^5-$C_5H_4SiMe_2OR_7Si_7O_{11}$-$\kappa^2O_2$)Cl] was prepared. The treatment of **1** with 1.0 equiv. of a triflate compound, $AgSO_3CF_3$ or $SiMe_3SO_3CF_3$ cleanly affords the triflate derivative [{Ti(η^5-$C_5H_4SiMe_2OR_7Si_7O_{11}$-$\kappa^2O_2$)}$(OSO_2CF_3)$] (**2**), as confirmed by NMR spectroscopy (Scheme 1).

Table 2
Myrcene polymerization with **1**/MMAO.

Entry	[Ti]/MMAO/My	T (°C)	Yield(%)[a]	M_w (Kg·mol^{-1})[b]	Đ
1	1/500/500	25	27	126.0	2.6
2	1/500/500	80	40	32.8	2.3
3	1/500/500	130	25	24.1	2.3
4	1/250/250	25	39	119.0	2.7
5	1/250/250	80	61	33.3	2.4
6	1/250/500	80	18	22.6	2.4
7	1/500/250	80	23	45.7	2.5

[a] General conditions: myrcene concentration = 0.6 m, amount of 1 = 58 μmol (116 μmol for entries 4, 5, and 7), solvent = toluene, and reaction time = 1 h a myrcene yield was determined gravimetrically.

[b] Experimental values of M_n and Đ obtained by GPC analysis, in THF and using polystyrene standards.

The formation of **2** is the result of the abstraction of the chloride ligand and the elimination of either AgCl or $SiMe_3Cl$ (Scheme 1), this latter compound was observed by ^{1}H NMR when the reaction was carried out in a sealed NMR tube. The resulting titanium compound was isolated in good yield (ca. 90%), and fully characterized by NMR and elemental analysis. Its spectroscopic behavior follows the same trends as those reported for its precursor **1** [22], confirming that the backbone ligand skeleton remains unaltered and agreeing with the proposed structure in Scheme 1. The more relevant spectroscopic features are the downfield shift for the fluorine atoms of the triflate group (at −77 ppm), in the ^{19}F NMR spectrum, indicating a weak interaction with titanium. However, the downfield shift of the resonances for **2** with respect to those found for **1** and its complete insolubility in toluene agrees with its expected cationic character.

Once **2** was synthesized and isolated, it was tested as catalyst for anethol polymerization. Its complete insolubility in toluene justifies its catalytic inactivity in such a solvent, however, when dichloromethane was used activity was observed. This is in agreement with the proposed cationic polymerization mechanism. All polymerization tests were thereafter performed in dichloromethane, adding the monomer at low temperature and then, allowing it to reach room temperature, beginning to measure the time from this moment.

The resultant polymers are amorphous, and showed bimodal molecular weight distributions (as measured by GPC, see Table 3). The latter aspect points towards the presence of two distinct active species, displaying different activities, with one producing high molecular weight PAN, which increases over time, and another producing low molecular weight PAN, which decreases over time [26]. However, the polydispersity of the two distinct polymers, remains, on the whole, constant (1.7–1.4 and 1.3–1.1, respectively) throughout the process.

To study the potential application of these biopolymers, the PMy from Table 2, entry 5, and the PAN from Table 3, entry 9 were chosen. Fig. 3 shows the thermal properties of the PMy, PAN, and pure PLA samples selected for this study. PMy and PAN samples are amorphous, and display very different T_g's. PMy shows a characteristically low T_g value, around – 73 °C, which, according to previous reports is a clear indication of its rubbery character [11,27–29]. In contrats, the PAN sample presents a very high T_g value, corresponding to a rigid polymer chain with aromatic groups, i.e., polystyrene family. The obtained DSC results show values ranging from 90 to almost 200 °C, due to the variation in the molecular weight. This result is interesting since, these polymers could be included in the group of those known as high T_g hydrocarbon polymers. This type of material is attracting increasing attention, due to interesting features such as, their high service temperature, low dielectric constant, non-hygroscopic nature and high transparency [30]. As an example of such materials, poly(1-phenyl-1, 3-butadiene) (PPB) is the hydrocarbon polymer featuring the highest T_g, of around 270 °C.

Fig. 3c shows the DSC traces at different heating rates obtained for the pure PLA sample during the second heating cycle. The PLA trace includes the glass transition (T_g around 60 °C), the cold crystallization process (above 100 °C) and the multiple melting peak (140–160 °C). The two endothermic peaks observed correspond to the melting of crystals with different stability and perfection. The explanation for this phenomenon is the melting of less perfect crystals that may originate from metastable crystal forms as well as thin lamellae and defects in the crystals. When the samples undergo cold-crystallization, they form imperfect crystals characterized by low stability [31,32]. With the increase in temperature during heating, these crystals melt giving rise to

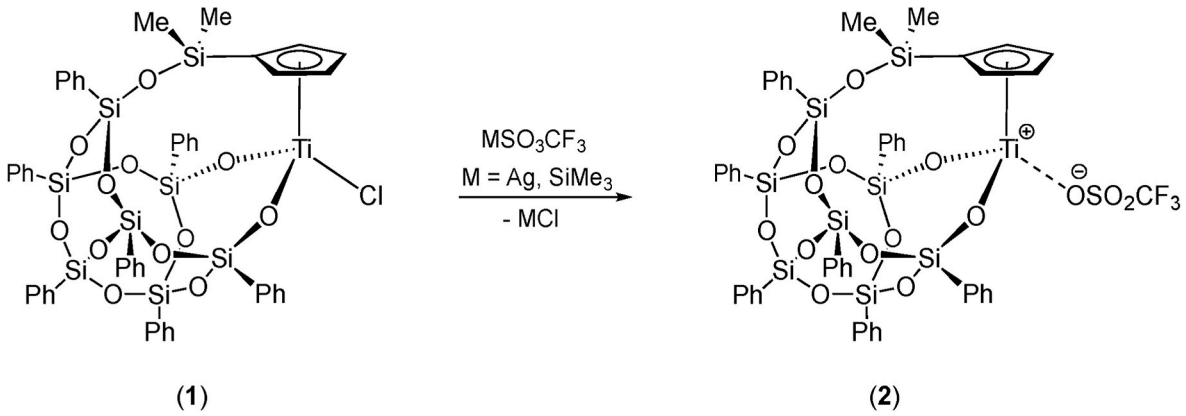

Scheme 1. Synthesis of the cationic triflate compound **2**.

Table 3
Anethole polymerization with compound **2**.

Entry	t (min)	Yield (%)[a]	M_w (Kg·mol^{-1})[b]	Đ[b]	ω (%)[c]
1	5	3	5.0	1.5	15.9
			138.0	1.3	
2	15	9	4.3	1.5	15.5
			189.0	1.4	
3	30	17	3.7	1.5	12.6
			252.4	1.5	
4	1 h	33	3.1	1.5	8.0
			702.0	1.2	
5	3 h	58	2.8	1.5	5.0
			1100.0	1.1	
6	5h	62	3.0	1.4	5.1
			1170.0	1.1	
7	7 h	64	2.9	1.5	4.8
			1208.5	1.1	
8	14 h	70	2.9	1.4	5.1
			954.2	1.1	
9	20 h	85	3.2	1.7	3.8
			1026.0	1.2	

General conditions: monomer concentration = 2 M, amount of **2** = 216 μmol, catalyst:anethol molar ratio 1:250, and solvent = dichloromethane. [a]Anethole yield was determined by gravimetric analysis, [b]Experimental values of M_n and Đ were determined by GPC analysis, in THF and using polystyrene standards, [c]w fraction of the high molecular weight chains was determined by integration of peak areas in SEC Chromatograms.

the first melting peak at the lowest temperature, though they may suffer a subsequent recrystallization. The second melting peak at the highest temperature corresponds to the melting of the crystals created during the recrystallization process. As is observed in Fig. 3c upon slow heating, rearrangement of the polymer molecules in the crystals occurs with a higher degree of perfection or thicker lamellae, as the additional peak moves to higher temperatures. Moreover, this additional peak grows at the expense of the melting peak at lower temperature, as the total enthalpic contribution, given by the difference $\Delta H = \Delta H_{cc} - \Delta H_m$, remains nearly constant at a value of 1.5–2.0 J g^{-1}. The above phenomena are associated with the process of improvement of crystal perfection/-thickness that was possible under the conditions of low heating rates.

Fig. 4 shows the DSC heating scans of PLA/PAN and PLA/PMy blends, after a previous cooling cycle at 10 °C·min^{-1}. The behaviour observed in the two series is clearly different, pointing to the definitively dissimilar nature of the second component. Firstly, it can be clearly observed that the T_g of the PLA component remains unchanged in the case of PLA/PAN systems. A very small decrease could be envisaged from the results in Fig. 4 for the blend with the highest PAN content. The T_g of the PAN phase is not discernible from the experimental results. Additionally, the cold crystallization – melting processes are closely supressed, and the crystal perfection/thickening already observed in pure PLA is absent in this series. On the contrary, in the case of PLA/PMy blends, a clear decrease of T_g is observed, and the cold crystallization – melting process is not supressed within the compositional range explored. Also, a decrease of the first melting peak temperature is obtained in this series (see Fig. 5).

The value of the total melting enthalpy, ΔH_m, remains almost constant within the compositional range explored. All the thermal properties (T_g, T_{cc}, T_m and ΔH_m) of the samples are listed in Table 4, and the evolution of the typical temperature transitions with the composition are plotted in Fig. 3. Thus, thermal analysis demonstrates that the introduction of a PMy into the PLA matrix leads to a reduction in both the glass transition temperature and the melting temperature of the crystals, and then to the PLA plasticization.

In summary, PAN and PMy cause important differences in the crystallization behaviour of PLA. The effect caused by the PAN sample is expected, as the glass transition (T_g = 96 °C) is even higher than that of the corresponding PLA (T_g = 56 °C). The rigid PAN sample does not permit the PLA molecular chains to crystallize at the selected cooling rate in the experiments (10 °C·min^{-1}), thus PAN does not plasticize nor nucleate the crystals of the more mobile PLA material. On the contrary, the very flexible PMy material, with a very low glass transition (T_g = −73 °C) effectively plasticizes the PLA, as its glass transition and melting temperature decreases in the mixtures. The cold crystallization process is not inhibited in this case by the presence of PMy in the mixture.

Crystallinity clearly decreases in the case of PLA/PAN blends, as DH decreases as PAN content increases. For PAN contents higher than 15 % no signs of crystallinity is detected in the DSC traces. In the case of PLA/PAN blends, the crystallinity remains around 2 % even for contents of PMyr as high as 12.5 %. The immiscible PAN clearly inhibits crystallization of PLA. On the contrary, the addition of PMyr, which is reported as partially miscible, does not affect to the crystallization of PLA.

Fig. 6 shows the TGA and the DTG curves of neat PLA and PAN as well as their blends, while the main results are summarized in Table 4. Neat PLA exhibited a one-step decomposition profile as is observed in Fig. 6b with a T_{max} around 350 °C. Similarly, the mass loss curve of neat PAN displays a single step of decomposition with a T_{max} close to 400 °C indicating that both polymers undergo a single degradation reaction, and that PLA has lower thermal stability that PAN. It has been previously reported that the thermal degradation of PLA is based on a transesterification reaction and chain homolysis which led to the production of different gaseous products such as cyclic oligomers, lactide, acetaldehyde, carbon monoxide and carbon dioxide [33]. On the other hand, PAN shows a thermal stability inherent to that of polystyrene probably with similar degradation mechanism involving the random scission of ester and aromatic groups to form intermediate radicals, which can leads to a drastic reduction of the molecular mass [34]. Moreover, regarding the DTG curves, the contribution of the thermal degradation of both homopolymers can be observed in the blends, this allows confirmation

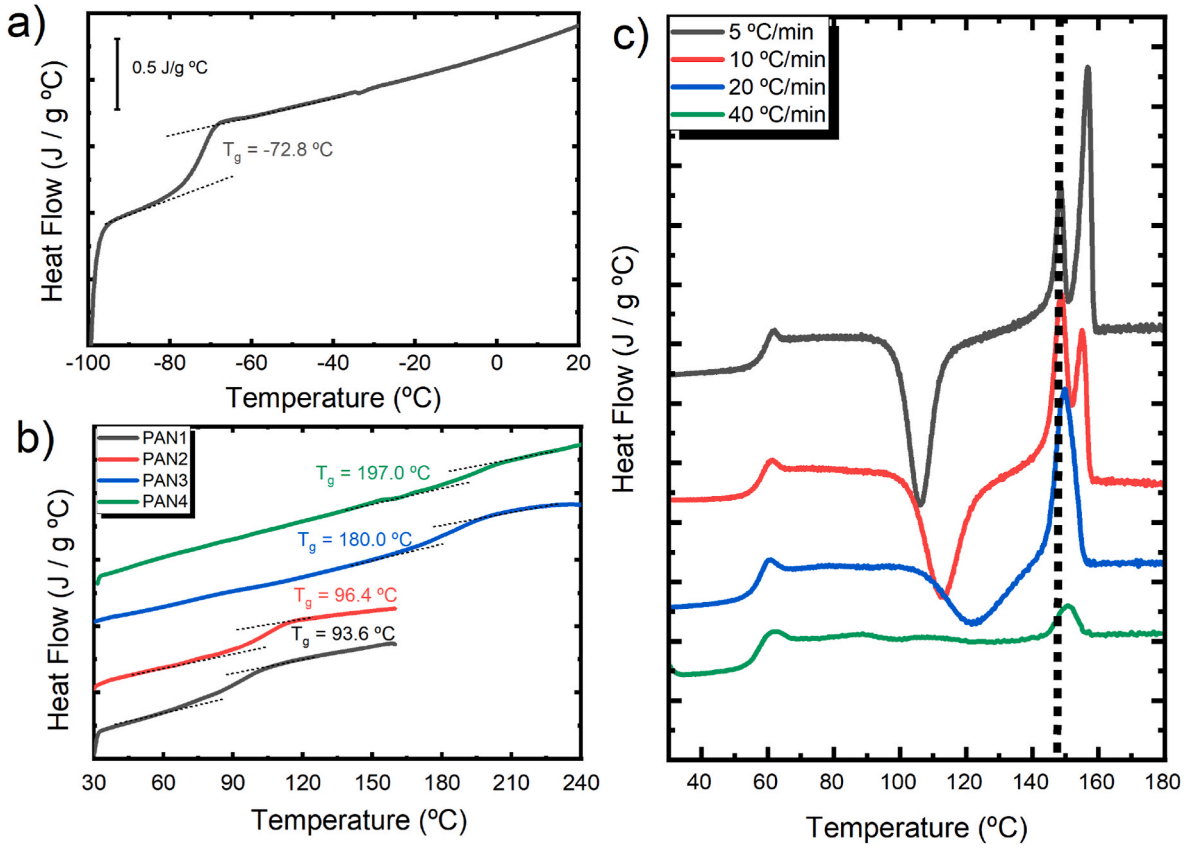

Fig. 3. DSC traces (second heating) obtained for the selected pure materials. PMy sample (a), PAN samples (b) and PLA sample (c). The PLA sample has been subjected to different heating rates using decreasing masses as heating rate increases to minimize thermal lag.

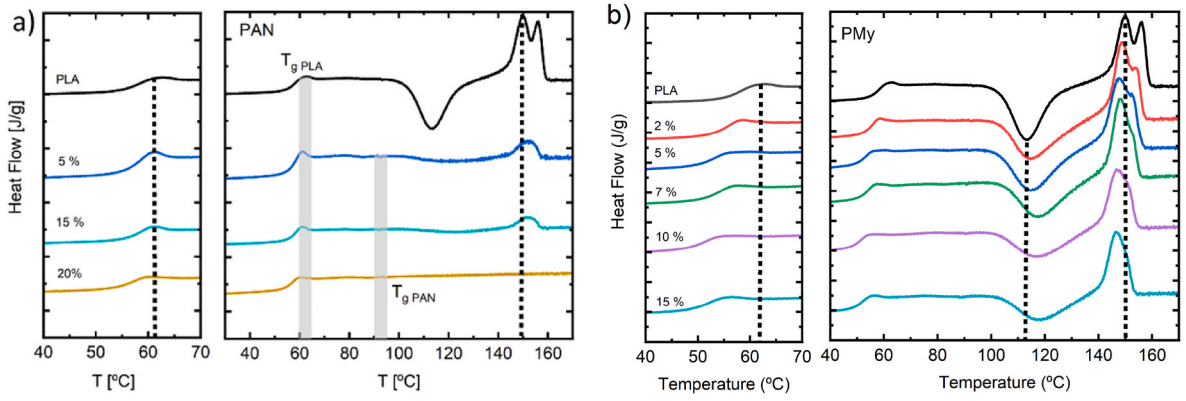

Fig. 4. DSC traces (second heating) obtained for the solution cast mixtures. PLA/PAN (a) samples and PLA/PMy (b) samples. In the left side of each panel, a zoom of the transition region is encompassed.

of the amount of each homopolymer in each of the distinct blends. The first degradation peak, at lower temperatures, can be attributed to the degradation of PLA while the second one to the degradation of the PAN present in the blend. Surprisingly, the peak related with PLA degradation in the blends appeared at lower temperature compared to that of pure PLA while the peak related with PAN degradation appears at similar temperature values (around 400 °C) for all the blends. Further, increasing the amount of PAN in the blends, the T_{max} related with PLA degradation remains unchanged while the $T_{5\%}$ decreases gradually. This is probably due to the effect of PAN on the crystallization process of PLA, inhibiting its crystallization, leading to a possible unfavorable thermal stability of the blends. However, such behavior could indicate a strong interaction between PLA and PAN confirming that the totally amorphous and rigid character of PAN can strongly affect the crystallization process of PLA as well as its kinetic and thermal properties. Similar behavior has been previously reported for PLA/polystyrene blends [35].

Fig. 7a and b shows the TGA and DTG curves of neat PLA, PMy and their blends. It can be observed from the DTG thermogram, the thermal decomposition of PMy occurred in a two-step degradation process. In particular, the sample weight loss gradually decreased from room temperature, until it reached around 350 °C, beyond which the rest of the polymer rapidly degraded. This is probably due to the polymeric microstructure which contains not only 1,4 microstructures, but also by a small amount of 3,4 structure, as detected by NMR. This mixture of leads to slightly different thermal stability of the polymeric chains. The

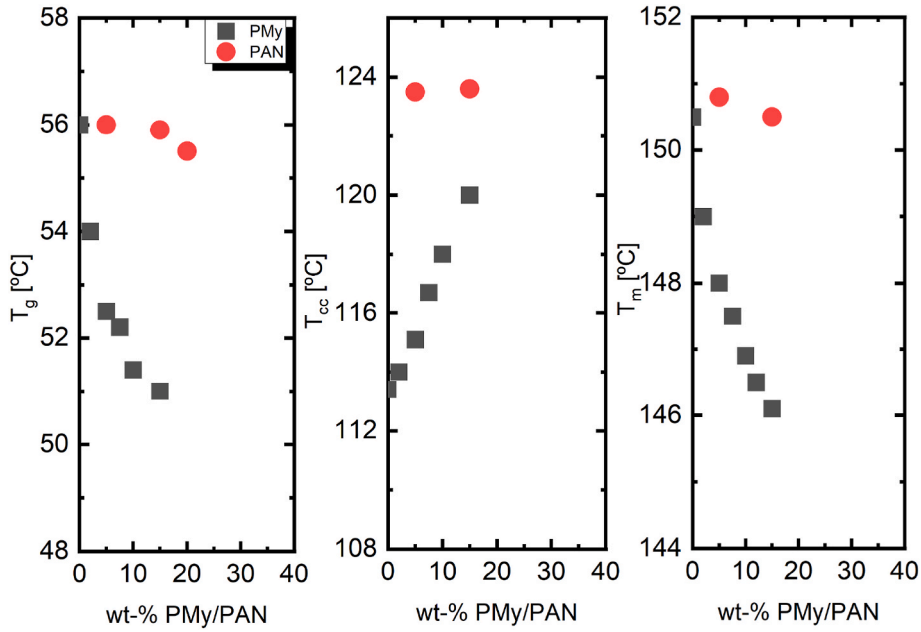

Fig. 5. Compositional dependence of the thermal transitions (T_g, T_{cc} and T_m) in the PLA/PAN and PLA/PMy mixtures.

Table 4
Thermal properties for all the mixtures in this study.

Sample	T_g (°C)	T_{cc} (°C)	T_m (°C)	ΔH (J/g)	X_c (%)	$T_{5\%}$ (°C)	T_{max} (°C)
PLA	56.0	113.4	150.0	2.0	2.1	307	349
PAN	96.0	–	–	–		260	393
PMy	−73.0	–	–	–		145	366/ 419
PLA5PAN	56.0	123.5	150.8	1.0	1.1	257	315/ 387
PLA15PAN	55.9	123.6	150.5	0.3	0.4	244	317/ 391
PLA20PAN	55.5	–	–	–		135	129/ 316/ 393
PLA2PMy	54.1	114.0	149.0	1.8	2.0	136	344
PLA5PMy	52.5	115.1	148.0	1.7	1.9	139	340
PLA7PMy	52.2	116.7	147.5	2.0	2.3	155	336
PLA10PMy	51.4	118.1	146.9	1.7	2.0	178	324
PLA12.5PMy	51.2	118.9	146.5	1.9	2.3	139	338
PLA15PMy	51.0	120.1	146.1	0.7	0.9	211	339

effect of the microstructures on the thermal behaviour of rubbers has already been reported for polybutadienes [36] and polymyrcenes [27, 37] and it is connected to the different reactivities of the various double bonds in the polymeric chains.

Compared with PLA, PMy showed higher thermal stability reaching a T_{max} of 366 and 419 °C. In Fig. 7 the contribution of the thermal degradation of both homopolymers can be observed in the PLA/PMy blends even if the peak related with the thermal degradation of PMy is not as clear as with the PLA/PAN blends. This likley indicates a better miscibility of PMy with PLA compared with PAN. Moreover, a first weight loss at low temperature (≈115 °C) was observed, probably due to the presence of water in the samples. Also, in this case, the peak related with PLA degradation in the blends appeared at lower temperature compare that of pure PLA indicating a decrease on the thermal stability of the PLA in the blends. This probably arises due to the already discussed effect of the microstructure on the thermal stability of the PMy that in some way leads to the drastic decrease of the $T_{5\%}$ values of the blends compared to that of pure PLA.

In Figs. 8 and 9, the SEM pictures of the surface of fracture of the original mixtures without any thermal treatment before and after etching clearly indicate the heterogeneous nature of the samples. The

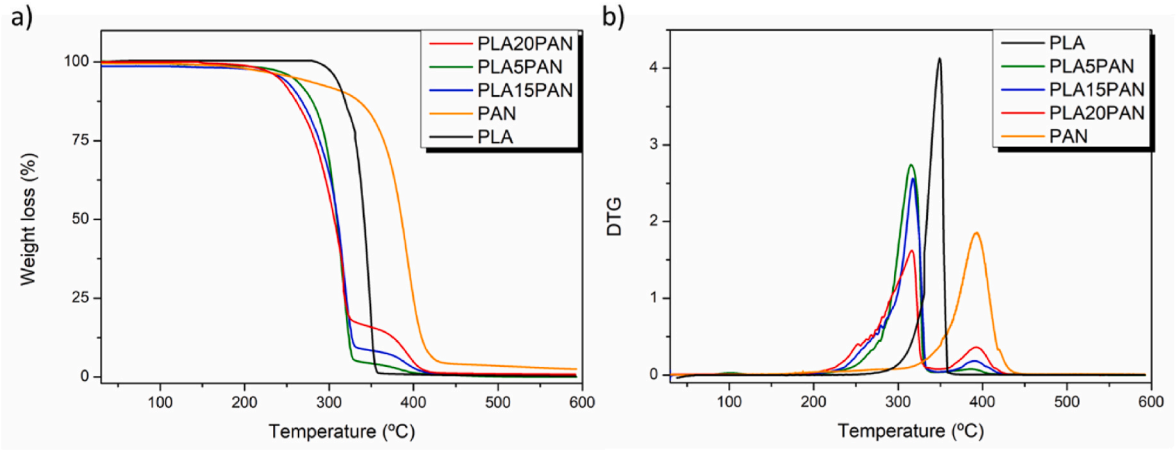

Fig. 6. TGA (a) and DTG (b) curves for the neat PLA and the different blends with PAN.

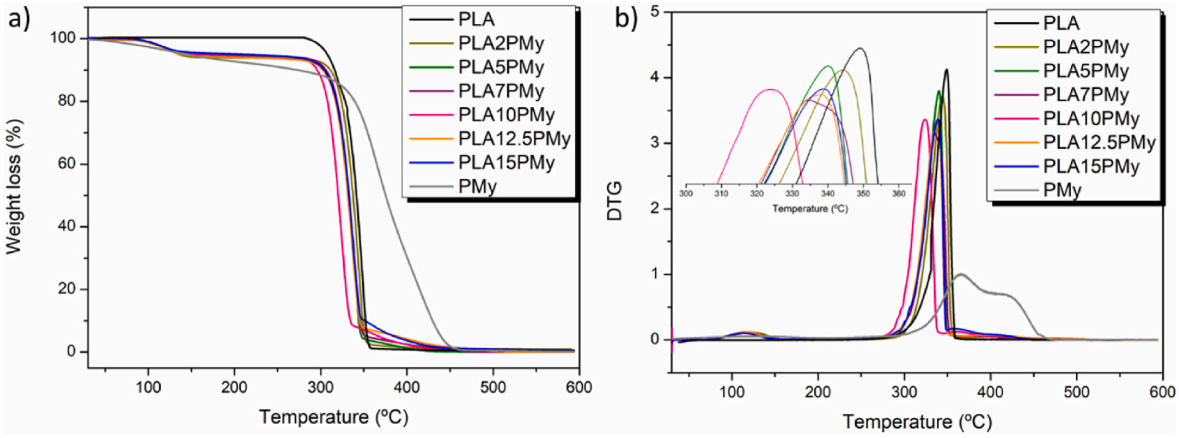

Fig. 7. TGA (a) and DTG (b) curves for the pure PLA and the different blends with PMy.

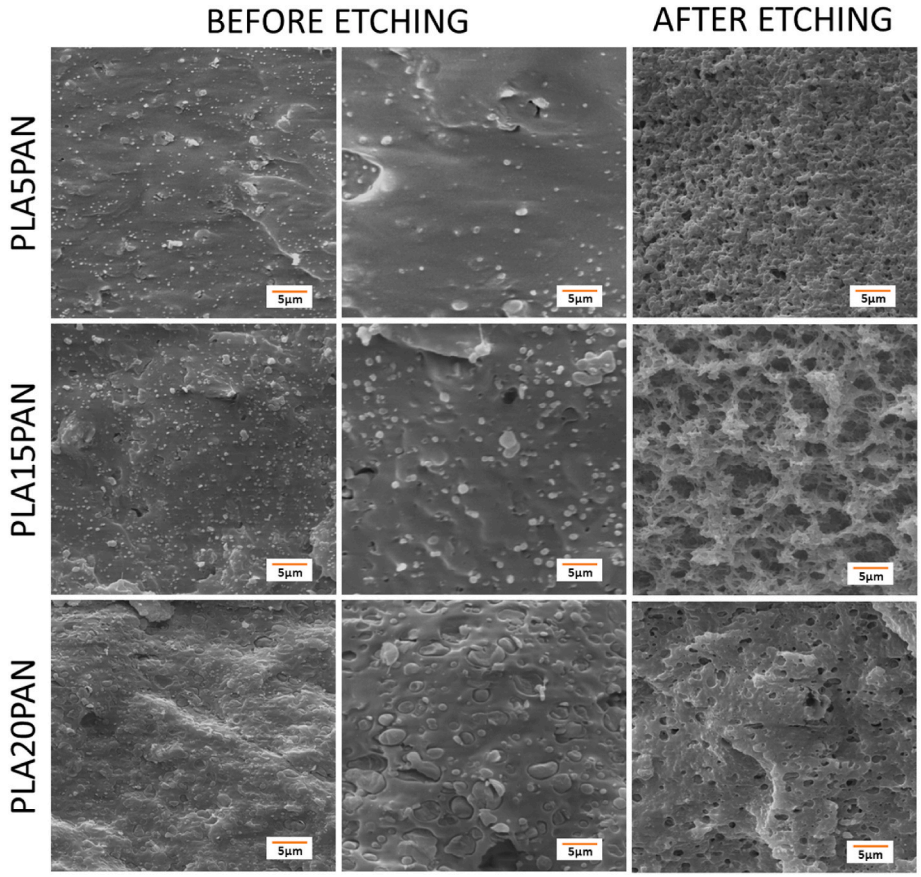

Fig. 8. SEM micrographs of all the PLA/PAN blends, before etching (left) and after etching (right) of PAN phase with xylene.

morphology is also different in PLA/PAN and PLA/PMy mixtures. In fact, well dispersed submicron size PAN domains are clear in the case of PLA/PAN mixtures, especially in the case of PLA/5PAN mixture. The PLA/PMy mixtures are different, as larger, but well dispersed, PMy domains are clearly visualized.

To reconcile this result with the thermal properties observed previously, it must be assumed that there is partial miscibility between PLA and PMy polymers. Another interesting observation that emerges from the observation of the images in Figs. 8 and 9 is the different domain size observed in both PLA/PAN and PLA/PMy mixtures. Solution cast mixing is a very well reported method for the preparation of thin films of polymeric mixtures, and phase separation upon solvent evaporation has been widely reported in immiscible systems. The final morphology in this type of systems depends on several factors: the support, the solvent and its evaporation rate, and the molecular weight of the involved species. In fact, previous works have reported that the domain size and the morphology strongly depend on the molecular weight of the dispersed phase [38,39]. The differences in domain size observed between PLA/PAN and PLA/PMy blends are clearly due to a distinct difference in the molecular weight of the PAN and PMy polymers. This specific behaviour has been reported on other immiscible or partially miscible systems.

We have additionally evaluated the mechanical properties of the thin films prepared from solution casting. The mechanical properties of such

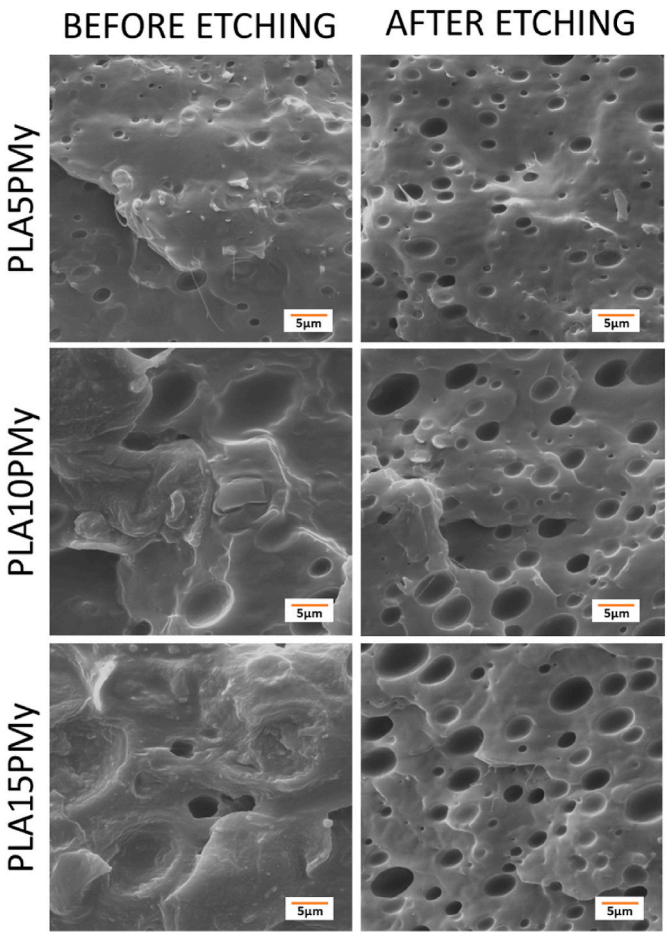

Fig. 9. SEM micrographs of all the PLA/PMy blends, before etching (left) and after etching (right) of PMy phase with hexane.

samples depend on their initial morphology (described by Figs. 9 and 11) and microstructure. The details of this microstructure may be understood from the DSC obtained from the first melting, using selected samples in Fig. 10a. The dependence of the dynamic tensile stress, σ*, with the dynamic strain, ε*, (dynamic stress-strain curves) at a frequency of 1 Hz in selected samples are shown in Fig. 10b. The results represent the average obtained from three independent measures in each sample. The dynamic tensile stress–strain curves show a large difference between the pure PLA sample and the blends.

From the results in Fig. 10a it can be seen that PLA molecules are able to crystallize during solvent evaporation in pure PLA and PLA/PMy blends. In these cases, the quantity of crystals is rather similar, as seen from the comparable value obtained for the melting enthalpy, ΔH, of around 21–22 J g^{-1}. On the contrary, the presence of PAN completely hampers PLA crystallization in PLA/PAN blends during solvent evaporation, as most of the crystals form during the cold crystallization process (the value of ΔH is around 1–2 J g^{-1}). These facts directly affect to the mechanical properties in Fig. 10b. The values for the slope for small values of the dynamic strain (linear region) directly give the dynamic tensile modulus, E*.

PLA displays a tensile modulus value of 1.80 GPa, very close to that reported for similar PLA films obtained from solvent casting [40]. The PLA/PMy sample in this study shows the typical behaviour associated with plasticization, as the tensile modulus decreases with the presence of PMy to a value of 1.25 GPa. Moreover, both PLA and PLA/PMy samples show the characteristic behaviour associated with plastic deformation of semicrystalline polymers, which gives rise to a deviation from the linear viscoelasticity for small values of dynamic strain. Low-M_w plasticizer behaves as solvent, leading to a decrease in the density of interactions amongst the PLA macromolecules. These results again point towards a certain level of miscibility between PLA and PMy. This plasticization effect is not present in PLA/PAN blends, as a clear increase in the elastic modulus is obtained up to values of around 1.90 GPa. This result points to a glassy nature of the PAN additive that gives rise to enhanced rigidity or elastic modulus, and the absence of plastic deformation within the dynamic strain explored. The plasticization effect in PLA/PMy blends

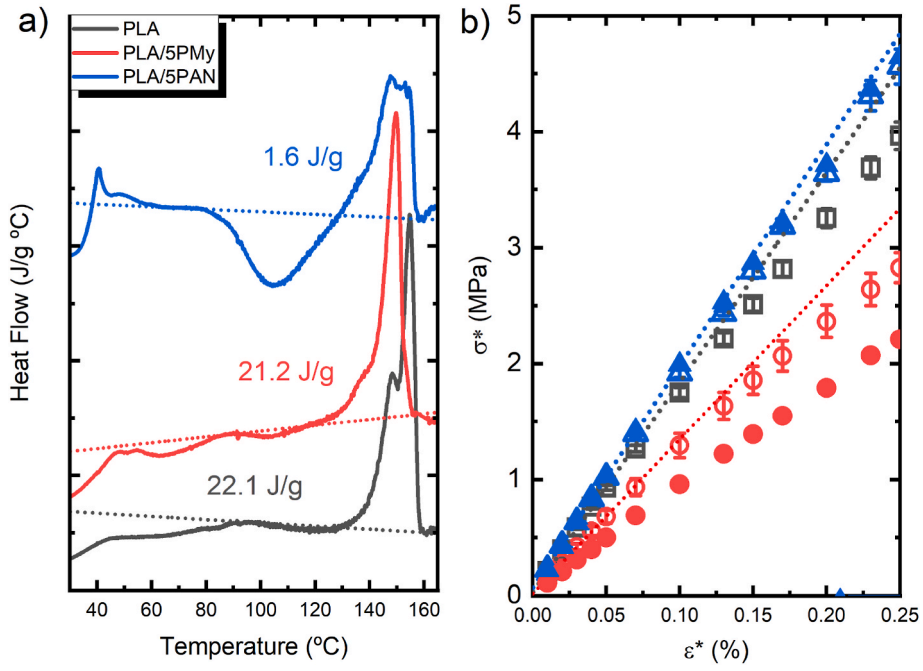

Fig. 10. a) DSC traces (first heating) of the PLA (black), PLA/5PMy (red) and PLA/5PAN (blue) samples and b) dynamic tension stress – strain curves at 1 Hz and room temperature of the same samples (open symbols). Additionally, the data obtained for PLA/15PMy and PLA/15PAN are included (solid symbols). The lines represent the linear viscoelastic zone to obtain the tensile modulus. (For interpretation of the references to colour in this figure legend, the reader is referred to the Web version of this article.)

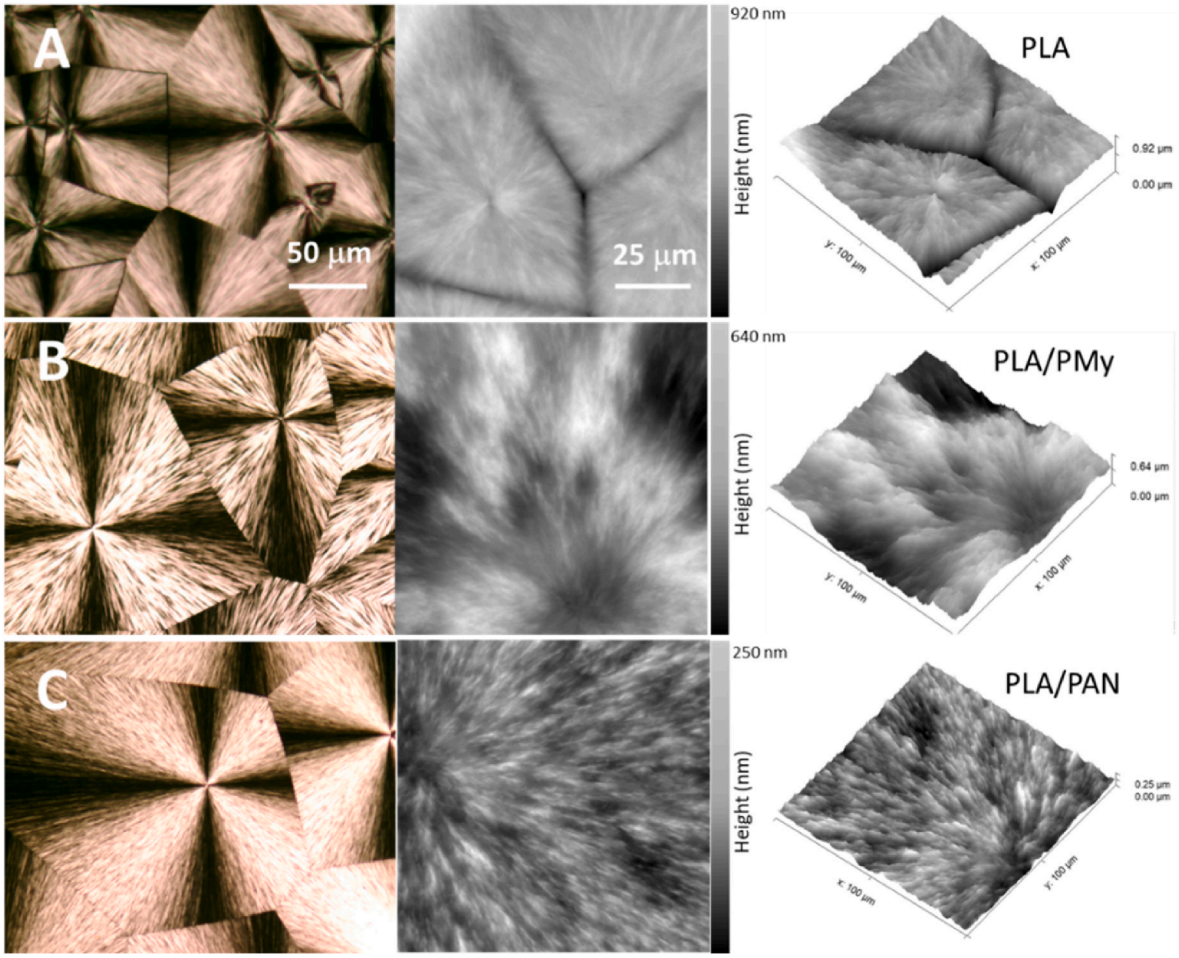

Fig. 11. POM (left) and AFM (right) of the spherulitic morphology of (A) PLA, (B) PLA/5PMy and (C) PLA/5PAN.

and the enhanced rigidity in PLA/PAN blends is more pronounced, as expected as the amount of PMy and PAN increases to 15 wt% (see Fig. 11b).

The morphology of pure PLA was compared to that of PLA blended with 5 wt% PyM and PAN. The morphological aspects are shown in Fig. 11 for films prepared by complete crystallization at T = 120 °C from the melt. The POM images (left) in Fig. 11 indicate the apparent absence of a ring-band pattern in the pure PLA (panel A) and the PLA/PAN blend (panel C). However, the addition of 5 wt% PyM to PLA alters the spherulitic morphology, as observed in panel B. The AFM height images (right) reveal an irregular ring-banded pattern in the centre of the spherulite in the PLA/PMy blend. The central panel clearly shows the bright and dark zones corresponding to ridges and valleys.

The AFM height profile shows that the distance between ridges is approximately 40–50 μm, and the height difference between the ridges and valleys is around 100–300 nm. Furthermore, intermediate ridges are present between the long ridges and the valleys. This hierarchical organization of the crystalline structure within the ridges and valleys suggests some type of segmental interaction and partial miscibility between the PLA and PMy. The appearance of ringed banded spherulites in blends due to the existence of interactions between the components has been widely reported, especially in the case of polyesters with polar diluents [41], including polycaprolactone (PCL) [42–44], and also in PLA [45]. Thus, the morphological features observed here in PLA/PMy blends may be caused by some type of segmental interaction and partial miscibility between the PLA and PMy.

4. Conclusions

A titanium complex with a tridentate silsesquioxanecyclopentadienyl ligand [Ti(η^5-$C_5H_4SiMe_2OPh_7Si_7O_{11}$-$\kappa^2O_2$)Cl] has been evaluated as a potential polymerization catalyst for bio-based monomers, such as β-myrcene and anethole. The resulting biobased polymers have been studied for the potential application as modifiers to enhance the properties of poly(lactic acid) (PLA).

When using myrcene and MMAO as co-catalyst, the titanium complex shows typical Ziegler-Natta behaviour. The resulting polymyrcene (PMy) exhibits 1,4-stereoregularity (90%, with 75% *cis* and 25% *trans*) and 3,4-stereoregularity (10%). In contrast, for anethol, a cationic mechanism is postulated as the active species has been observed to be a triflate salt of the titanium compound. It is notable that the obtained polyanethol (PAN) is atactic.

When PMy is blended with PLA, the bio-based additive acted as a plasticizer, resulting in a decrease in T_g and promotion of PLA crystallization when a PMy content below 15 wt% was applied. Morphology analysis indicated a partially miscible, phase-separated system with micron-sized domains. The mechanical properties of the blends also showed plasticization, with decreased elastic modulus and enhanced plasticity, resulting in less fragile systems compared to pure PLA. The micron-sized domains were consistent with a high molecular weight PMy samples.

In contrast to PMy, PAN completely inhibited PLA crystallization and the PLA/PAN blends were immiscible, but a well-dispersed, phase-separated system was obtained in solvent-casting film preparation with very small PAN domains. The small domains could be attributed to the

low molecular weight of the PAN sample. The blends show higher tensile modulus and hardness than PLA and an absence of plastic behaviour. Thus, an increased rigidity is generated upon the addition of PAN to PLA.

Overall, this study highlights the potential of the titanium complex with a tridentate silsesquioxanecyclopentadienyl ligand as a catalyst to produce bio-based polymers, which can be used as modifiers for PLA. The findings also provide insights into the effects of PMy and PAN on the properties and morphology of PLA blends, which can provide important information for the future development of renewable and sustainable materials.

CRediT authorship contribution statement

Joan Vinueza-Vaca: Investigation, Writing – review & editing. **Emma Franco-Mateo:** Investigation. **Valentina Sessini:** Investigation, Writing – review & editing. **Marta E. G. Mosquera:** Funding acquisition, Project administration, Writing – review & editing. **Virginia Souza-Egipsy:** Investigation. **Javier Ramos:** Investigation, Writing – review & editing. **Juan F. Vega:** Investigation, Writing – review & editing. **Gerardo Jiménez:** Funding acquisition, Project administration, Conceptualization, Supervision, Writing – original draft, Writing – review & editing. **Vanessa Tabernero:** Conceptualization, Supervision, Investigation, Writing – original draft, Writing – review & editing.

Declaration of competing interest

The authors declare the following financial interests/personal relationships which may be considered as potential competing interests: Vanessa Tabernero reports financial support was provided by Universidad de Alcalá. Vanessa Tabernero reports a relationship with University of Alcala that includes: funding grants.

Data availability

No data was used for the research described in the article.

Acknowledgements

The authors would like to thank the financial support from the Ministerio de Ciencia e Innovación and Agencia Estatal de Investigación (Spain) through the project PID2021-122708OB-C31, PID2019-107710 GB-I00, TED2021-130871B–C22, and RYC2021-033921-I, Project UAH-AE-2017-2. J.M.V. thanks the Universidad de Alcalá for FPI-572765 Predoctoral Fellowship and the PIUAH21/CC-028 project. The TEM-BIOPHYM Service at the IEM-CSIC is acknowledged for granting the use of the facilities.

Appendix A. Supplementary data

Supplementary data to this article can be found online at https://doi.org/10.1016/j.polymer.2023.126494.

References

[1] A.K. Mohanty, F. Wu, R. Mincheva, M. Hakkarainen, J.-M. Raquez, D.F. Mielewski, R. Narayan, A.N. Netravali, M. Misra, Sustainable polymers, Nat. Rev. Methods Prim. 2 (1) (2022) 46, https://doi.org/10.1038/s43586-022-00124-8.

[2] D. Notta-Cuvier, J. Odent, R. Delille, M. Murariu, F. Lauro, J.M. Raquez, B. Bennani, P. Dubois, Tailoring polylactide (PLA) properties for automotive applications: effect of addition of designed additives on main mechanical properties, Polym. Test. 36 (2014) 1–9, https://doi.org/10.1016/j.polymertesting.2014.03.007.

[3] V. Sessini, M. Palenzuela, J. Damián, M.E.G. Mosquera, Bio-based polyether from limonene oxide catalytic ROP as green polymeric plasticizer for PLA, Polymer 210 (2020), 123003, https://doi.org/10.1016/j.polymer.2020.123003.

[4] R.P. Quirk, Triblock polymers of a monovinyl aromatic compound and myrcene, U. S. Patent No. 4 374 (957) (1983).

[5] R.A. Newmark, R.N. Majumdar, 13C-NMR spectra of cis-polymyrcene and cis-polyfarnesene, J. Polym. Sci., Part A: Polym. Chem. 26 (1) (1988) 71–77, https://doi.org/10.1002/pola.1988.080260107.

[6] D.L. Trumbo, Free radical copolymerization behavior of myrcene, Polym. Bull. 31 (6) (1993) 629–636, https://doi.org/10.1007/BF00300120.

[7] J. González-Villa, E. Saldívar-Guerra, R.E.D. de León-Gómez, H.R. López González, J.R. Infante-Martínez, Kinetics of the anionic homopolymerizations of ß–myrcene and 4–methylstyrene in cyclohexane initiated by n–butyllithium, J. Polym. Sci., Part A: Polym. Chem. 57 (21) (2019) 2157–2165, https://doi.org/10.1002/pola.29487.

[8] M.I. Hulnik, I.V. Vasilenko, A.V. Radchenko, F. Peruch, F. Ganachaud, S.V. Kostjuk, Aqueous cationic homo- and co-polymerizations of β-myrcene and styrene: a green route toward terpene-based rubbery polymers, Polym. Chem. 9 (48) (2018) 5690–5700, https://doi.org/10.1039/C8PY01378K.

[9] D.H. Lamparelli, M. Winnacker, C. Capacchione, Stereoregular polymerization of acyclic terpenes, ChemPlusChem 87 (1) (2022), e202100366, https://doi.org/10.1002/cplu.202100366.

[10] C.S. Marvel, C.C.L. Hwa, Polymyrcene, J. Polym. Sci. 45 (145) (1960) 25–34, https://doi.org/10.1002/pol.1960.1204514503.

[11] R.E. Díaz de León Gómez, F.J. Enríquez-Medrano, H. Maldonado Textle, R. Mendoza Carrizales, K. Reyes Acosta, H.R. López González, J.L. Olivares Romero, L.E. Lugo Uribe, Synthesis and characterization of high cis-polymyrcene using neodymium-based catalysts, Can. J. Chem. Eng. 94 (5) (2016) 823–832, https://doi.org/10.1002/cjce.22458.

[12] R.N. Kularatne, A. Yang, H.Q. Nguyen, G.T. McCandless, M.C. Stefan, Neodymium catalyst for the polymerization of dienes and polar vinyl monomers, Macromol. Rapid Commun. 38 (19) (2017), 1700427, https://doi.org/10.1002/marc.201700427.

[13] J. Wang, S. Xu, X. Hu, Y. Huo, X. Shi, Rare-earth metal complexes bearing pyridyl-functionalized amidinate ligands for highly trans-1,4-selective living (Co) polymerization of 1,3-conjugated dienes, Organometallics 41 (2) (2022) 115–123, https://doi.org/10.1021/acs.organomet.1c00557.

[14] S. Loughmari, A. Hafid, A. Bouazza, A. El Bouadili, P. Zinck, M. Visseaux, Highly stereoselective coordination polymerization of β-myrcene from a lanthanide-based catalyst: access to bio-sourced elastomers, J. Polym. Sci., Part A: Polym. Chem. 50 (14) (2012) 2898–2905, https://doi.org/10.1002/pola.26069.

[15] T. Higashimura, Y. Hirokawa, K. Matsuzaki, T. Kawamura, T. Uryu, Cationic polymerization of anethole and its model reaction: a stereochemical approach to the propagation mechanism, Polym. J. 11 (11) (1979) 855–862, https://doi.org/10.1295/polymj.11.855.

[16] K. Nomura, J. Liu, S. Padmanabhan, B. Kitiyanan, Nonbridged half-metallocenes containing anionic ancillary donor ligands: new promising candidates as catalysts for precise olefin polymerization, J. Mol. Catal. Chem. 267 (1) (2007) 1–29, https://doi.org/10.1016/j.molcata.2006.11.006.

[17] J. Schellenberg, N. Tomotsu, Syndiotactic polystyrene catalysts and polymerization, Prog. Polym. Sci. 27 (9) (2002) 1925–1982, https://doi.org/10.1016/S0079-6700(02)00026-6.

[18] M. Mateos, J. Vinueza, M.E.G. Mosquera, V. Tabernero, T. Cuenca, G. Jiménez, Cyclopentadienyl-silsesquioxane titanium compounds as suitable candidates for immobilization on silica-based supports, Inorg. Chim. Acta. 501 (2020), 119275, https://doi.org/10.1016/j.ica.2019.119275.

[19] M. Ventura, M.E.G. Mosquera, T. Cuenca, B. Royo, G. Jiménez, Cyclopentadienyl–silsesquioxane titanium complexes: highly active catalysts for epoxidation of alkenes with aqueous hydrogen peroxide, Inorg. Chem. 51 (11) (2012) 6345–6349, https://doi.org/10.1021/ic300583g.

[20] Y. Zhu, C. Romain, C.K. Williams, Sustainable polymers from renewable resources, Nature 540 (7633) (2016) 354–362, https://doi.org/10.1038/nature21001.

[21] M. Maiza, M.T. Benaniba, G. Quintard, V. Massardier-Nageotte, Biobased additive plasticizing Polylactic acid (PLA), Polimeros 25 (2015) 581–590, https://doi.org/10.1590/0104-1428.1986.

[22] L. Postigo, M. Ventura, T. Cuenca, G. Jiménez, B. Royo, Selective sulfoxidation with hydrogen peroxide catalysed by a titanium catalyst, Catal. Sci. Technol. 5 (1) (2015) 320–324, https://doi.org/10.1039/C4CY00965G.

[23] D. Garlotta, A literature review of poly(lactic acid), J. Polym. Environ. 9 (2) (2001) 63–84, https://doi.org/10.1023/A:1020200822435.

[24] C.A. Mahieux, Environmental Degradation of Industrial Composites, Elsevier, 2005.

[25] a) D. Takeuchi, T. Aida, Sequential cationic and anionic polymerizations by triflate complexes of bulky titanium bisphenolates: one-pot synthesis of Polyoxetane−Poly(ε-caprolactone) block copolymer, Macromolecules 33 (13) (2000) 4607–4609, https://doi.org/10.1021/ma000377p;
b) D.H. Lamparelli, M.M. Kleybolte, M. Winnacker, C. Capacchione, Sustainable myrcene-based elastomers via a convenient anionic polymerization, Polymer 13 (2021) 838–845, https://doi.org/10.3390/polym13050838.

[26] a) M.I. Hulnik, O.V. Kuharenko, I.V. Vasilenko, P. Timashev, S.V. Kostjuk, Quasiliving cationic polymerization of anethole: accessing high-performance plastic from the biomass-derived monomer, ACS Sustain. Chem. Eng. 9 (19) (2021) 6841–6854, https://doi.org/10.1021/acssuschemeng.1c01504;
b) M.I. Hulnik, O.V. Kuharenko, P. Timashev, I.V. Vasilenko, S.V. Kostjuk, AlCl3×OPh2-Co-initiated cationic polymerization of anethole: facile access to high molecular weight polymers under mild conditions, Eur. Polym. J. 165 (2022), 110983, https://doi.org/10.1016/j.eurpolymj.2021.110983;
c) J.M. Rooney, Cationic polymerization of anethole by triphenylmethyl hexafluoroantimonate, Makromol. Chem. 179 (10) (1978) 2419–2430, https://doi.org/10.1002/macp.1978.021791008.

[27] P. Sarkar, A.K. Bhowmick, Synthesis, characterization and properties of a bio-based elastomer: polymyrcene, RSC Adv. 4 (106) (2014) 61343–61354, https://doi.org/10.1039/C4RA09475A.
[28] J. Hilschmann, G. Kali, Bio-based polymyrcene with highly ordered structure via solvent free controlled radical polymerization, Eur. Polym. J. 73 (2015) 363–373, https://doi.org/10.1016/j.eurpolymj.2015.10.021.
[29] P. Sahu, A.K. Bhowmick, Redox emulsion polymerization of terpenes: mapping the effect of the system, structure, and reactivity, Ind. Eng. Chem. Res. 58 (46) (2019) 20946–20960, https://doi.org/10.1021/acs.iecr.9b02001.
[30] Y. Cai, J. Lu, G. Jing, W. Yang, B. Han, High-glass-transition-temperature hydrocarbon polymers produced through cationic cyclization of diene polymers with various microstructures, Macromolecules 50 (19) (2017) 7498–7508, https://doi.org/10.1021/acs.macromol.7b01075.
[31] M.L. Di Lorenzo, Calorimetric analysis of the multiple melting behavior of poly(L-lactic acid), J. Appl. Polym. Sci. 100 (4) (2006) 3145–3151, https://doi.org/10.1002/app.23136.
[32] R. Lv, Y. He, J. Wang, J. Wang, J. Hu, J. Zhang, W. Hu, Flash DSC study on the annealing behaviors of poly(l-lactide acid) crystallized in the low temperature region, Polymer 174 (2019) 123–129, https://doi.org/10.1016/j.polymer.2019.04.061.
[33] H. Zou, C. Yi, L. Wang, H. Liu, W. Xu, Thermal degradation of poly(lactic acid) measured by thermogravimetry coupled to Fourier transform infrared spectroscopy, J. Therm. Anal. Calorim. 97 (3) (2009) 929–935, https://doi.org/10.1007/s10973-009-0121-5.
[34] R. Appiah-Ntiamoah, H. Kim, B.T. Gadisa, A.F. Baye, M.W. Abebe, S.V. Kostjuk, Degradation kinetics of polyanethole: a newly synthesized green polymer, Mater. Chem. Phys. 219 (2018) 468–477, https://doi.org/10.1016/j.matchemphys.2018.08.061.
[35] A. Mohamed, S.H. Gordon, G. Biresaw, Poly(lactic acid)/polystyrene bioblends characterized by thermogravimetric analysis, differential scanning calorimetry, and photoacoustic infrared spectroscopy, J. Appl. Polym. Sci. 106 (3) (2007) 1689–1696, https://doi.org/10.1002/app.26783.
[36] M.P. Luda, M. Guaita, O. Chiantore, Thermal degradation of polybutadiene, 2. Overall thermal behaviour of polymers with different microstructures, Makromol. Chem. 193 (1) (1992) 113–121, https://doi.org/10.1002/macp.1992.021930111.
[37] N. Bauer, J. Brunke, G. Kali, Controlled radical polymerization of myrcene in bulk: mapping the effect of conditions on the system, ACS Sustain. Chem. Eng. 5 (11) (2017) 10084–10092, https://doi.org/10.1021/acssuschemeng.7b02091.
[38] E. Jalali Dil, P.J. Carreau, B.D. Favis, Morphology, miscibility and continuity development in poly(lactic acid)/poly(butylene adipate-co-terephthalate) blends, Polymer 68 (2015) 202–212, https://doi.org/10.1016/j.polymer.2015.05.012.
[39] J.-M. Widmaier, G. Mignard, Polystyrene-poly(α-methylstyrene) blends: influence of molecular weight on miscibility, Eur. Polym. J. 23 (12) (1987) 989–992, https://doi.org/10.1016/0014-3057(87)90046-2.
[40] C. Echeverría, I. Limón, A. Muñoz-Bonilla, M. Fernández-García, D. López, Development of highly crystalline polylactic acid with β-crystalline phase from the induced alignment of electrospun fibers, Polymers 13 (17) (2021) 2860, https://doi.org/10.3390/polym13172860.
[41] H.D. Keith, F.J. Padden Jr., T.P. Russell, Morphological changes in polyesters and polyamides induced by blending with small concentrations of polymer diluents, Macromolecules 22 (2) (1989) 666–675, https://doi.org/10.1021/ma00192a027.
[42] D. Ma, J. Zhang, M. Wang, J. Ma, X. Luo, The comparison of the ringed spherulite morphology of PCL blends with poly(vinyl chloride), poly(bisphenol A carbonate) and poly(hydroxyether of bisphenol A), Macromol. Chem. Phys. 202 (7) (2001) 961–966, https://doi.org/10.1002/1521-3935(20010401)202:7<961::AID-MACP961>3.0.CO;2-Q.
[43] H. Yiping, L. Xiaolie, M. Dezhu, Ringed spherulite morphology and compatibility in the binary blends of poly(ε-caprolactone) with ethyl cellulose, Eur. Polym. J. 37 (10) (2001) 2153–2157, https://doi.org/10.1016/S0014-3057(01)00032-5.
[44] C.-C. Su, J.-H. Lin, Ringed spherulites in ternary polymer blends of poly (ε-caprolactone), poly(styrene-co-acrylonitrile), and polymethacrylate, Colloid Polym. Sci. 283 (2) (2004) 182–193, https://doi.org/10.1007/s00396-004-1119-y.
[45] H. Ni'mah, E.M. Woo, S.-M. Chang, Composite banded core and non-banded shell transition patterns in stereocomplexed poly(lactide acid) induced by strongly interacting poly(p-vinyl phenol), RSC Adv. 4 (99) (2014) 56294–56301, https://doi.org/10.1039/C4RA09859E.